Published in final edited form as:
Nat Chem Biol. 2017 September ; 13(9): 975–981. doi:10.1038/nchembio.2434.

Structures of carboxylic acid reductase reveal domain dynamics underlying catalysis

Deepankar Gahloth[#1], **Mark S. Dunstan**[#1], **Daniela Quaglia**[1,$], **Evaldas Klumbys**[1], **Michael P. Lockhart-Cairns**[2,3], **Andrew M. Hill**[1], **Sasha R. Derrington**[1], **Nigel S. Scrutton**[1], **Nicholas J. Turner**[1], and **David Leys**[1]

[1]Manchester Institute of Biotechnology, School of Chemistry, University of Manchester, 131 Princess Street, M1 7DN Manchester, UK

[2]Division of Cell Matrix Biology and Regenerative Medicine, School of Biological Sciences, University of Manchester, Oxford Road, M13 9PT Manchester, UK

[3]Diamond Light Source, Harwell Science & Innovation Campus, Didcot, OX11 ODE, Oxfordshire, UK

[#] These authors contributed equally to this work.

Abstract

Carboxylic acid reductase (CAR) catalyzes the ATP- and NADPH-dependent reduction of carboxylic acids to the corresponding aldehydes. The enzyme is related to the non-ribosomal peptide synthetases, consisting of an adenylation domain fused via a peptidyl carrier protein (PCP) to a reductase termination domain. Crystal structures of the CAR adenylation–PCP didomain demonstrate that large-scale domain motions occur between the adenylation and thiolation states. Crystal structures of the PCP–reductase didomain reveal that phosphopantetheine binding alters the orientation of a key Asp, resulting in a productive orientation of the bound nicotinamide. This ensures that reduction of the aldehyde product does not occur. Combining crystallography with small-angle x-ray scattering (SAXS), we propose that molecular interactions between initiation and termination domains are limited to competing PCP docking sites. This is supported by the fact that (*R*)-pantetheine can support CAR activity for mixtures of the isolated domains. Our model suggests directions for further development of CAR as a biocatalyst.

[$]present address: Département de chimie, Université de Montréal 2900, Boulevard Édouard-Montpetit, Montréal, Québec, Canada, H3T 1J4.

Contributions

MD cloned, expressed and purified various CAR enzymes (both truncations and full-length as well as hybrid forms) and obtained crystal structures for both A and R domains. DG cloned, expressed and purified various CAR enzymes and obtained crystals structures for the PCP-didomain constructs in addition to isolated R domain structures. DG and MPL performed SAXS data collection and modeling. E.K., D.Q., A.M.H and S.R.D. performed kinetic data analysis. All authors discussed the results and participated in writing of the manuscript. N.J.T., N.S.S and D.L. initiated and directed this research.

Competing financial interests

The authors declare no competing financial interests.

Europe PMC Funders Author Manuscripts

Introduction

The ATP- and NADPH-dependent reduction of carboxylic acids to the corresponding aldehydes is catalyzed by the bacterial carboxylic acid reductase (CAR) enzymes [1–3]. These enzymes consists of an adenylation domain fused via a peptidyl carrier protein (PCP) to a reductase termination domain, and are related to the nonribosomal peptide synthetases (NRPS) [4–7]. CAR enzymes show substantial promise as green biocatalysts for the conversion of aromatic and short chain carboxylic acids into the corresponding aldehydes [3]. Individual CARs have been shown to convert a wide range of substrates, featuring in applications that range from the conversion of long-chain fatty acids into fuel precursors [8–12], to the production of starting materials for cascade reactions that generate enantiomerically pure chiral building blocks [13] (Supplementary Results, Supplementary Fig. 1). Newly characterized CAR family members continue to expand this synthetic chemistry toolbox [14]. However, unlocking the catalytic potential of these enzymes is hampered by the lack of mechanistic and structural insights. CAR represents a distant relation of the NRPS family, lacking any extension module (Fig. 1a). In fact, CAR consists of a substrate-activating adenylation domain more closely related in substrate specificity and sequence to the acyl-CoA synthetase members of the ANL superfamily of adenylating enzymes [15]. While the latter enzymes generate CoA thioester products, the CAR adenylation domain is fused to a PCP domain, and thus resembles the NRPS initiator (or adenylation) module with respect to the thioester product. The similarity with the modular NRPS enzymes extends to the inclusion of a terminator domain in CAR: an aldehyde-product-releasing reductase domain is fused to the acyl-intermediate carrier PCP. While sequence similarity of the CAR adenylation domain with known structures is limited to ~20%, closely related reductase structures (~50 % similarity to CAR) from NRPS enzymes are available [16,17]. However, these enzymes catalyze the progressive 4-electron reduction of the PCP-bound acyl group to the corresponding alcohol. In contrast, CAR catalyzes a strictly 2-electron reduction, releasing the corresponding aldehyde product (Fig. 1a).

To provide detailed understanding of the CAR mechanism, we determined the crystal structure of individual CAR domains, both with and without the PCP domain. A range of CARs was screened for crystallization, and structural data could be obtained for enzymes from *Nocardia iowensis*, *Mycobacterium marinum* and *Segniliparus rugosus*. Combining the crystallographic structures with SAXS studies, we reveal that large-scale domain dynamics underpin catalysis in CAR. Furthermore, we reveal that docking of the phosphopantetheine group in the reductase active site leads to reorientation of the nicotinamide moiety of bound NADPH from a non-catalytic to a catalytically competent position. We propose that this ensures reduction does not proceed beyond the aldehyde product, and show that mutagenesis of a single Asp residue involved in the nicotinamide reorientation leads to modest formation of the 4-electron-reduced alcohol product.

Results

Structure of and substrate binding by the CAR A domain

To understand the key determinants underpinning substrate specificity and the mechanism of acyl-AMP formation, we determined the structure of the adenylation domains (A domains)

of CAR from *Nocardia iowensis* (CAR*ni*) and *Segniliparus rugosus* (CAR*sr*). In each case, the structure was obtained in complex with AMP that remained tightly bound during purification (Fig. 1b). The AMP is bound at the A domain center, establishing an extensive network of molecular contacts conserved across the ANL superfamily [15,18]. Most similar structures include the bacterial benzoate-CoA ligase [19] and the human medium-chain acyl-coenzyme A synthetase ACSM2A [20] (Supplementary Fig. 2a). Previous studies on these enzymes and other members of the ANL superfamily have revealed the presence of a mobile C-terminal domain (A_{sub}, residues 527-654) that adopts distinct positions correlated to the specific reactions catalyzed. Domain motion has been inferred from structures with distinct nucleotide ligands, with the ATP-bound form representing the adenylation state of the enzyme, and AMP or AMP-acyl bound forms frequently observed bound to the thiolation state [15]. For both CAR A domain structures, the exact orientation of the A_{sub} domain is highly similar and, despite containing AMP, is more akin to ANL structures that correspond to the adenylation state. The universally conserved Lys from ANL motif A10 [18] in the A_{sub} domain (K629 in CAR*sr*) makes contact with the nucleotide ligand (a hallmark of the adenylation state), while the conserved A8 Gly [18] (located close to the AMP-acyl substrate in the thiolation state; G532 in CAR*sr*) is directed away from the active site (Supplementary Fig. 2a). The P-loop that grips the terminal ATP phosphates is disordered in CAR*sr* while adopting a position wedged in between the A_{core} (residues 1-526) and the A_{sub} domains in CAR*ni*. In both CAR A domain structures, the domain interface established between A_{sub} and the N-terminal A_{core} domain is more extensive when compared with other ANL enzymes in the adenylation state. This suggests the conformational equilibrium of the isolated CAR A_{sub} domain remains poised towards the adenylation state, apparently unaffected by the nature of the nucleotide ligand.

The acid substrate binding site is identified by benzoic acid bound to CAR*ni* and an unidentified molecule (modeled as fumarate) present close to the AMP phosphate that was co-purified with CAR*sr* (Fig. 1c). Most of the relatively narrow substrate binding pocket is lined by hydrophobic residues, with His300 (conserved in CAR enzymes; H315 in CAR*sr*) located close to both AMP phosphate and the substrate carboxylate. The active site volume of CAR*sr* is smaller due to the presence of Phe294 (Ser280 in CAR*ni*), and distinct in shape due to insertion of Ala425 in CAR*ni*. The substrate specificity of these enzymes was determined by screening against a diverse carboxylic acid substrate panel including benzoic, heterocyclic, phenylacetic/propanoic and fatty acid substrates (Supplementary Fig. 1). *Para*- and *meta*- substituted benzoic acids, such as toluic acid, show high levels of activity against several CAR enzymes. All CARs tested exhibited a poor tolerance for *ortho*- substituents, presumably due to steric hindrance.

The CAR A–PCP didomain is a dynamic entity

To explore whether the A_{sub} conformation is affected by the presence of the PCP domain, and establish how the thioester linkage between the acyl-AMP and the PCP phosphopantetheine is formed, we determined the structure of the CAR*sr* adenylation–PCP region (A–PCP). The latter could be crystallized in two distinct conformations that differ in the position of the A_{sub} and PCP domains. While one A_{sub} domain conformation is similar to that previously observed for the single A domain (i.e. the adenylation state; Fig. 2a,b), a

second, distinct conformation was observed in a different crystal form (Fig. 2c,d). In the adenylation state, the PCP domain is positioned distant from the A domain, the A_{sub}–PCP linker region adopting an extended alpha-helical conformation. The PCP Ser702 that serves as the phosphopantetheine attachment site is positioned 52 Å away from the bound AMP phosphate. In contrast, the relative orientation of both PCP and A_{sub} domains has altered in the second A–PCP crystal structure, with the Ser702–AMP phosphate distance dramatically shortened to 19 Å. This large reduction in distance is the cumulative effect of two distinct domain re-orientations. The adenylation A_{sub} domain has reoriented via a rotation of ~165 degrees at the A8–Lys528 hinge region, although the A_{sub} center of gravity remains largely in place. Both the position of the hinge and extent of rotation resemble the motion seen between the adenylation and thiolation conformations in other ANL family members [5,6,15](Fig. 2; Supplementary Fig. 2b). The relative orientation of the PCP domain and the A_{sub} domain has also changed, with an additional ~75 degree rotation at Ala651 leading to the more dramatic PCP domain reorientation. The cumulative effect of both the Lys528 and Ala651 rotations is a displacement for the PCP domain center of gravity by ~50 Å. The reorientation of both PCP and A_{sub} domains leads to a structure compatible with thiolation (Fig. 2d). Although phosphopantetheine is not present in our structure, an overlay with the related initiation module of NPRS LgrA [7] reveals a very similar orientation of the PCP relative to the A_{core} domain, with the phosphopantetheine linker accommodated by a narrow channel lined with conserved consensus sequence elements from the A_{sub} domain (Supplementary Fig. 2b).

In addition to the altered A_{sub}–A_{core} domain interaction of the thiolation conformation, a new domain interaction surface is established between the PCP domain and the A_{core} domain, overlapping in part with the adenylation A_{sub}–A_{core} domain interaction (Supplementary Fig. 3). The presence of this additional interaction is therefore likely to affect the adenylation–thiolation conformational equilibrium of the A_{sub} domain when comparing the isolated A domain with the A-PCP didomain region. Biophysical parameters for the CAR*sr* A-PCP in solution were determined by SAXS, multi-angle light scattering (MALS) and area under the curve (AUC) analysis (Supplementary Fig. 4). Neither of the crystal structures obtained correlated well with the experimental data. Rigid-body modeling using both linker regions (K528 and A651) resulted in an ensemble of two models that accounted for the SAXS profile, one resembling the A–PCP thiolation state crystal structure and the other corresponding to an open conformation of the A_{sub} domain not observed in the crystal structures. These data are consistent with the expected flexibility of the A–PCP didomain. While the observed position of the PCP domain in the adenylation state is influenced by crystal lattice contacts (a total of ten putative hydrogen bonding interactions can be observed between the PCP domain and symmetry-related monomers), the conformation seen in the crystal structure is likely one of a wider range of possible conformations the A–PCP didomain can adopt in solution.

CAR R domain structures reveal an on-off equilibrium

We sought to complement our understanding of the CAR A–PCP didomain by determining the structure of the CAR reductase (R) domain. In particular, we wanted to determine how this domain ensures that further reduction of the aldehyde product does not occur. Crystal

structures of the reductase domains from CAR*sr* and CAR*mm* (*Mycobacterium marinum*) reveal that this region is highly similar in structure to the terminal reductase domains of other NPRS [16,17], albeit with a distinct orientation of the smaller substrate binding domain (Fig. 3a). Furthermore, crystals could be readily obtained in a variety of crystal forms. For CAR*mm*, these reveal that two distinct conformations of Asp984 (Asp998 in CAR*sr*) in the reductase active site can occur, corresponding to active and inactive forms of the reductase, respectively (Fig. 3b). In the active form, the nicotinamide moiety is ordered and placed adjacent to conserved residues Thr921 and Tyr956. The latter are proposed to form the oxyanion hole that assists in reduction of the thioester [21]. Asp984 is positioned pointing away from the nicotinamide, buried within the protein matrix and hydrogen bonding to Asp1034. This conformation is similar to that observed for the 4-electron reductase from MxaA [17] (Supplementary Fig. 5). In contrast, Asp984 adopts a distinct conformation in the majority of the CAR*mm* reductase monomers (similar to the Asp998 conformation observed for CAR*sr* reductase), leading to a disordered nicotinamide moiety and thus inactive state. This disorder is a consequence of the fact that Asp984 and the Ser983 carbonyl group are located within the nicotinamide binding pocket. The motion of Asp984 between both conformations is concomitant with reorientation of the backbone of residues 983–985. Comparison of the various CAR*mm* reductase structures reveals that the latter appears to be linked to the position of the smaller substrate binding domain. This suggests a possible means by which CAR ensures reduction does not proceed beyond the aldehyde product: binding of the substrate-thioester PCP affects the position of the substrate binding domain, and hence the conformational equilibrium of Asp984. The latter appears poised towards the inactive state in the absence of the PCP-acyl substrate. In contrast, the aldehyde product might lack sufficient binding affinity to affect this equilibrium. Recently studied polyketide synthase (PKS) enzymes containing reductase off-loading domains implicated in aldehyde (as opposed to alcohol) production also contain an Asp residue at the corresponding position [22,23]. However, one of these does further reduce the aldehyde product to alcohol in the absence of a suitable transaminase to the trap the transient aldehyde intermediate [22]. The conformational equilibrium between on- and off-state in the CAR R domain extends beyond Asp984 reorganization, including the backbone reorientation of residues 983–985. Hence, the presence of an Asp984-equivalent residue might not in itself be sufficient to determine the product scope. In the case of CAR*sr*, while mutation of the equivalent Asp998 to Gly does not appear to affect benzoic acid reduction rates, it does lead to formation of the modest levels of the alcohol product *in vitro* (Supplementary Fig. 6). Furthermore, in contrast to the WT CAR, the CAR*sr* D998G variant displays modest benzaldehyde reductase activity. This suggests that Asp998 is required to ensure strict 2-electron reductase activity by CAR, and that the R domain has little affinity for the isolated benzaldehyde (as opposed to the covalently linked benzoyl-phosphopantetheine moiety). The physiological substrate(s) of CAR is unknown, and it is possible that Asp998 is required to ensure 4-electron reduction does not occur for the corresponding aldehydes.

A phosphopantetheine binding-induced activation mechanism

In order to verify our hypothesis, we determined the crystal structure of the CAR*sr* PCP–reductase (PCP–R) didomain. As observed for the isolated reductase domains, crystals could be readily obtained in the presence of NADPH, and a variety of crystal forms could be

obtained. The PCP domain is clearly visible in the corresponding crystal structures, and adopts a conformation independent of crystal packing, presenting the first crystal structure for an intact PCP–R didomain (Fig. 3c). The PCP domain is docked onto the larger NADPH binding domain, directly above the ribose 2'-phosphate binding pocket, with no direct contacts established to the smaller substrate binding domain. This suggests that binding of the adenosine 2'5'-diphosphate moiety of NADPH is likely to precede PCP docking, with reorganization of the nicotinamide group linked to phosphopantetheine binding. The PCP phosphopantetheine linker Ser702 is located 16 Å from the nicotinamide binding pocket. In the unmodified CAR*sr* PCP–R structure, the bound NADPH nicotinamide remains disordered with Asp984 observed in the inactive conformation. In contrast, the crystal structure of the CAR*sr* PCP–R modified with phosphopantetheine reveals an active conformation (Fig. 3d,e). In the latter, the smaller substrate binding domain has reoriented slightly to establish contacts between the phoshopantetheine group and the P1013–Q1015 region, in turn leading to reorientation of the Y966 loop region from the larger NADPH-binding domain with concomitant active site closure. A plausible model for the reductase acyl-PCP complex is made by extending the phosphopantetheine arm with a benzoyl moiety. This directly places the substrate acyl group above the pro-*S* H on the C4 nicotinamide, in agreement with observed kinetic isotope effects (KIE; Supplementary Figs. 5 and 9a,b). It also reveals that few, if any, interactions are made between the R domain and the benzoyl moiety. The ~50-fold decrease in NADPH oxidation levels upon providing benzoyl-CoA as a substrate instead of benzoic acid and ATP (i.e. bypassing the A domain) reveals that the increase in effective concentration of the thioester substrate by covalent tethering is an important factor in achieving high enzyme activity (Table 1). However, no activity could be observed with thiobenzoic acid, confirming that thioester substrate affinity is largely dependent on the phosphopantetheine linker region as opposed to the benzoyl moiety. This also provides a likely explanation for the modest reductase activity observed with benzaldehyde in the case of the CAR*sr* D998G variant. In addition, the free phosphopantetheine thiol group itself represents a steric hindrance to aldehyde binding directly above the nicotinamide. The latter is demonstrated both by the fact that the *apo* form of CAR*sr* D998G (i.e. unmodified with phosphopantetheine) displays higher benzaldehyde reduction activity compared to the *holo* CAR*sr* D998G, and by the fact the presence of free phosphopantetheine inhibits benzaldehyde reduction observed for either of these variants (Table 1).

Mutation of residues involved in establishing contacts between the R domain and the phoshopantetheine group abolish CAR activity (Supplementary Fig. 5d). This strongly suggests the presence of the substrate-phosphopantetheine itself is required to induce Asp 984–Ser 985 reorientation and concomitant reductase activation. This is supported by the fact that benzoyl-CoA can act as a substrate for the isolated CAR*sr* R domain and R–PCP didomain. To prove that the (*R*)-pantetheine moiety itself is required for activation of the R domain, we tested for benzoic acid reductase activity of a CAR*sr* S702A mutant in the presence of (*R*)-pantetheine or a similarly sized thiol. Only the addition of (*R*)-pantetheine was able to rescue CAR activity for the S702A variant, confirming that free (*R*)-pantetheine can bypass the lack of PCP Ser702-bound phosphopantetheine group for the A domain, resulting in formation of a benzoyl-pantetheine thioester that can serve as a substrate for the

R domain. Biophysical parameters for the unmodified CAR*sr* PCP–R didomain in solution were determined by SAXS, MALS and AUC analysis, revealing that neither of the crystal structures obtained correlate well with the experimental data (Supplementary Fig. 7). Rigid-body modeling using S744 as a linker region revealed that an ensemble of multiple PCP–R conformations accounted for the SAXS profile obtained. This suggests a highly dynamic nature of the PCP domain in solution, in accordance with the relatively small interaction surface observed in the PCP–R crystal structure.

Modeling of the full-length CAR reveals a dynamic entity

Armed with the various crystal structures of the distinct CAR*sr* PCP-containing regions, we modeled the full-length CAR (Fig. 4). While the A–PCP structure in the thiolation mode is clearly incompatible with the available PCP–R structures (the PCP cannot be simultaneously docked to both the respective partner domains), an overlay of the adenylation A–PCP conformation (i.e. PCP-off) with the modified PCP–R (i.e. PCP-on) reveals only minor clashes occur between the adenylation and reductase domains (Fig. 4a). The latter are easily avoided by minimal reorientation of the A_{sub}–PCP Ala651 hinge region. An overlay of the thiolation state A–PCP structure with the PCP–R SAXS-derived models reveals a very distinct model for the full-length enzyme (Fig. 4b).

To verify the dynamic nature of CAR, we determined the solution structure of CAR*sr* using SAXS (Supplementary Fig. 8). Neither of the models presented in Figure 4a,b account for the observed SAXS profile, and rigid-body modeling using four domains linked by the three identified hinge regions (K528, A651 and S744) reveals that two distinct conformations, both representing an open conformation of the enzyme, can account for the observed profile (Fig. 4c; Supplementary Fig. 8). The addition of ATP and/or $NADPH_4$ (a reduced version of NADPH) did not substantially alter the scattering behavior of the sample. This therefore suggests that the dynamic equilibrium between the various conformations of the full-length enzyme is not poised towards either the adenylation/reduction or thiolation conformations, but likely randomly explores various conformations, some relevant with respect to catalysis, others for ligand exchange. Substantial solvent viscosity effects on CAR catalytic efficiency support this hypothesis (Supplementary Fig. 9c,d).

Domain-exchanged CARs retain activity

While mixtures of isolated CAR domains do not display benzoic acid reductase activity, the addition of free (*R*)-pantetheine can support CAR activity in such mixtures (Table 1). This confirms that neither covalent linkage between individual domains nor the presence of a PCP domain is an absolute prerequisite for activity. Hence, this suggests CAR enzyme activity is not inextricably linked to the exact nature of the covalent linkage between the individual CAR domains nor to the respective interdomain surface contacts. Hence, this robust dynamic nature of CAR suggests that domain exchange to produce novel hybrid CARs should be feasible. Similar domain-exchange experiments carried out on NPRS systems have met with some success [24–27]. To test our hypothesis we exchanged domains from CAR*ni* and CAR*mm* to create nmCAR and mnCAR hybrids. Interestingly, both hybrids showed activity towards a range of diverse substrates (Supplementary Fig. 10). Further studies will be required to determine the extent by which the respective A and R

domains determine substrate specificity, but our present data suggests that the A domain is the key determinant.

Discussion

The reduction of carboxylic acids to the corresponding aldehydes is a relatively simple reaction, but often suffers from the inadvertent production of alcohol by-products through further reduction of the aldehyde product under the conditions used. The bacterial carboxylic acid reductase is able to catalyze the strictly 2-electron reduction of a range of carboxylic acids using ATP and NADPH. CAR enzymes offer tremendous potential for future applications in organic synthesis, particularly with respect to generating aldehydes from carboxylic acids under mild reaction conditions. Moreover, as recently demonstrated [13], CARs can be combined with other enzymes (e.g. transaminases, imine reductases) in cascade processes, thereby enabling the conversion of simple, inexpensive starting materials to products with greater functionality and complexity. Such cascades will increasingly require engineered CARs with broad substrate scope and activity for the synthesis of a wide range of target molecules.

Our crystallographic and solution characterization of CAR suggests an intricate mechanism that ensures reduction of the carboxylic acid substrate is restricted to the aldehyde level. Crystal structures of the isolated reductase domain reveal two distinct conformations of the active site region, only one of which appears catalytically competent (i.e. the “on” state) by virtue of the fact the nicotinamide moiety is in close proximity to the conserved Thr and Tyr involved in catalysis. However, the latter is only apparent in small subset of the available reductase domain monomer structures, with the majority adopting an “off” state that has a disordered nicotinamide binding mode. The on–off conformational equilibrium thus appears poised towards the off-state for the isolated reductase domain, and is largely centered around the reorientation of a key Asp residue located close to the nicotinamide. Substrate binding, which in this case can be considered to be the acyl-phosphopantetheine-PCP domain, can affect this equilibrium, leading to substrate-induced enzyme activation. The latter has been observed in a wide range of enzymes, and often forms an integral part of those systems that contain inherently dangerous activities from the cellular perspective (i.e. proteases [28], kinases [29], and NAD^+-dependent ADP-ribosyltransferases [30]). Substrate-induced active site remodeling offers a suitable safeguard in such cases.

In the case of CAR, the structures of the PCP–R didomain in the presence and absence of the phosphopantetheine modification reveal that active site remodeling occurs as a direct consequence of an induced-fit phosphopantetheine docking in the reductase active site cleft and not the PCP-domain itself. This is supported by the fact that benzoyl-CoA can act as a substrate. Although the CAR R domain key Asp that is affected in position by the induced fit of the pantetheine moiety is present in other terminal reductase domains [22,23], it remains unclear whether this represents a more general mechanism to control reduction activity.

In contrast to the intricate activation of the reductase domain, the communication and transfer of the activated acyl group appears to depend on a relatively simple and robust system consisting of a beads-on-a-string type of arrangement (Fig. 5). The overlay of the

Europe PMC Funders Author Manuscripts

adenylation A–PCP conformation with the modified PCP–R structure presents a putative model for the full-length CAR*sr* structure when in the adenylation/reduction conformation (Fig. 4a). This also suggests that reduction of the substrate-phosphopantetheine linkage might occur simultaneously with activation of the next substrate molecule in the adenylation domain, although a scenario whereby these reactions occur sequentially [6] remains equally likely. A putative model for the thiolation state of the full-length CAR is assembled by combining the thiolation A–PCP crystal structure (i.e. PCP-on) with the PCP–R SAXS models (i.e. PCP-off, Fig. 4b). This reveals that a dramatic reorientation of the reductase domain with respect to the adenylation is required for the transition from the adenylation/reduction conformation to the thiolation conformation. Crucially, a comparison of both models clearly suggests the absence of a long-lived interaction between the CAR terminal domains. The SAXS models of the full length enzyme present a dynamic picture with the various domains sampling the conformational space available (Fig. 4c). Hence, the enzyme appears to function as a highly mobile entity that makes use of competing docking sites for the PCP domain on the A_{core} and reductase domains. This is consistent with the lack of ATP- and benzoic acid-dependent NADPH consumption activity when adding either CAR A domain with the cognate PCP–R fragments (Table 1). The lack of interactions and/or sophisticated communication between the CAR terminal domains suggests that the CAR catalytic repertoire can be diversified by domain exchange with the CAR family as we demonstrate here. A similarly robust design was recently uncovered for intermodular communication in hybrid PKS–NRPS [31], underpinning the engineering of polyketide-nonribosomal peptide interfaces [32]. By analogy, this suggests the possibility to explore new chemistry by fusion of CAR domains with appropriate NRPS components in future. The fact that free (*R*)-pantetheine can be used to support the activity of isolated domains suggests it might even be possible to bypass the need for covalent linkage between these components. It also confirms that the A domain can catalyze ATP-dependent formation of acyl-pantetheine in the absence of the PCP domain, reminiscent of the related acyl-CoA ligase activity [19]. Hence, while the isolated A and R domain are functional in the presence of (*R*)-pantetheine, the increase in effective concentration arising from covalent tethering to the PCP domain is a substantial contributor to the efficiency of the natural system.

Online methods

Cloning and molecular biology

All FL-CAR enzymes were cloned into pET28b using Infusion® HD Cloning technology to give a N-terminal His-tag. The experiment was designed *in silico* using the SnapGene software and pET28-b vector linearized using the restrictions sites *NdeI* and *EcoRI*. Individual CAR domains and their boundaries were identified with the software MOTIF scan and PSI-blast searches. Sequence alignments with known NRPS modules were used to select the final domain boundaries for cloning. Truncated CAR constructs containing just N-terminal domains were designed and cloned with a N-terminal His-tag and C-terminal CAR domains with a C-terminal His-tag. Individual CAR domains were cloned using the same protocol adopted for FL-CARs accept *NcoI* was used instead of *NdeI* for N-terminal constructs. For CAR*sr* constructs, DNA corresponding to CARsr Full-length (FL), Adenylation (A), Adenylation-PCP (A-PCP), PCP-Reductase (PCP-R) and Reductase (R)

was amplified by PCR from the *CARsr* gene. PCR products were cloned into the Ligation independent cloning site of pNIC28a-Bsa4 vector using the ligation-independent method (Infusion HD, Clontech). These constructs have N-terminal His-tag and Tobacco Etched Virus (TEV) protease cleavage site followed by amino acid sequence. Sequence of all the constructs were verified by DNA sequencing (Eurofins). Point mutations in CARsr were introduced by Q5® site-directed mutagenesis kit (NEB).

Protein expression and purification

Expression and purification of CAR*mm/ni* and *sr* enzymes and individual (di)domain. *E. coli* BL21 (DE3) were transformed with one or two plasmids: a pET28-b containing FL-CAR or containing the individual CAR domains, and where modification with phoshopantetheine was required (for activity studies and/or crystallography), a second vector, pCDF1b-Sfp, containing the gene for the expression of Sfp: phosphopantetheine transferase from *Bacillus subtilis*. A single colony was then used to inoculate 5 mL of LB medium containing 50 μg/mL streptomycin (only where the pCDF1b-Sfp vector was present) and kanamycin, and grown overnight, shaking at 37 °C. For CAR*mm/ni* expression, the inoculum was transferred and grown to mid-log phase in 2 L baffled flasks, containing TB medium, induced with 0.4 mM IPTG and shaken for 24 hours at 20 °C. Proteins were purified to homology using Nis60 Ni resin (Clontech) followed by size exclusion chromatography with a prep grade 26/60 Hi-load Superdex S200 purification column. Final samples were eluted in 25 mM Tris pH 8.0 and 150 mM NaCL.

For expression and purification of the CAR*sr* constructs (FL, A, A-PCP, PCP-R and R), cultures were incubated at 37 °C to an optical density (OD_{600}) between 0.6-0.8, and protein expression was induced with 0.1 mM IPTG at 20 °C for 16 h. Cells were harvested by centrifugation and stored in -80 °C until further use. For purification, cells were re-suspended in Ni-binding buffer (20 mM HEPES pH 7.4, 0.5 M NaCl, 10 mM Imidazole) supplemented with EDTA-free protease inhibitor cocktail tablet (Sigma). The cells were lysed by cell-disruptor followed by centrifugation at 48,000 ×g for 1h. Cleared supernatant was loaded on to equilibrated Ni-NTA agarose resin (Qiagen) and final elution was done with 250 mM imidazole. Affinity His-tag was removed by TEV protease cleavage at 4 °C. Cleaved protein was passed back over the Ni-NTA agarose beads and flow-through was collected. Cleaved protein was further cleaned by ion-exchange chromatography using the ResQ (6ml) column (GE healthcare). Protein was eluted in a linear gradient of NaCl (0-1 M). Protein-containing fractions were pooled together and concentrated up to ~10 mg/ml with 10 K MWCO (Vivaspin) filtration unit.

In vitro modification of CAR*sr* PCP-R by Sfp

CAR*sr* PCP-R didomain was modified by promiscuous phosphopantetheinyl transferase Sfp according to the method described previously [33]. In brief, 0.1 μM purified Sfp was mixed with 5 μM of PCP-R protein and 5 μM benzoyl-CoA (Sigma) in 50 mM HEPES pH 7.5 and 10 mM $MgCl_2$ in total 100 μl volume. This reaction mixture was incubated at room temperature minimum for 2h. In order to remove Sfp, the mixture was separated using gel-filtration.

Screening for CAR activity

The activity of FL-CAR towards a range of carboxylic acids was tested by following the reduction of NADPH at 340 nm over 1 min. Measurement were performed using a Tecan infinite M200 pro 96 wells plate spectrophotometer fitted with an injector. Seven alternative CARs were tested using the following conditions: 0.15 mM NADPH 1 mM ATP, 10 mM $MgCl_2$, 5 mM substrate, 2.5% DMSO (for substrate solubility) in 50 mM Tris-HCl pH 7.5, room temperature.

The reactions were tested in 96 well plates using a total volume of 200 μL per well. The amount of enzyme used for each reaction was constant (5 μL). The enzyme was pre-pipetted in the wells and the rest of the reaction mix injected in each well just before the measurement started. Each measurement ran for 1 minute and the slope was then calculated using the Magellan software considering the variation in absorbance between 3 s and 12 s, over 10 points of measure: this allowed for elimination of the mixing effect observed occasionally just after injection and allowed for measurement of the activity of the enzymes in the linear range. All measurements were corrected with an appropriate blank. All measurements were generally repeated in quadruplicate and at least in triplicate for each sample. The substrates tested are reported in Supplementary Fig. 1.

Activity assays for individual N-terminal domains were carried out with the commercially available EnzChek assay kit and 1 mM ATP, 10 mM $MgCl_2$, 5 mM substrate and 50 mM Tris-HCl pH 7.5. Reactions were monitored for the conversion of 2-amino-6-mercapto-7-methylpurine riboside (MESG) by purine nucleoside phosphorylase (PNP) to ribose 1-phosphate and 2-amino-6-mercapto-7-methyl- purine at 360 nm over 15 minutes.

Substrate dependent NADPH oxidation activity of CARsr (FL, ACP-R, R, A+ACP-R as well as variants) was monitored by NADPH consumption at 340 nm. Assays were carried out in 50 mM Tris-Cl pH 7.5, 150 mM NaCl, 10 mM $MgCl_2$, 1 mM ATP, 1 mM NADPH, 5mM of respectively benzoic acid, benzoyl-CoA or thiobenzoate. The effect of R-pantetheine, decanethiol and pentanethiol on substrate dependent NADPH oxidation was assessed by addition to 2mM final concentration of these compounds. Activity assays using benzaldehyde as a substrate were carried out using a similar protocol, but with 15 mM of benzaldehyde as final concentration.

Crystallization and Structure determination

Crystals of A domain CAR*ni* (30mg/ml) were obtained using the sitting-drop vapour-diffusion and grew within 7 days at 4 °C in 0.12 M ethylene glycols 0.1 M Tris-Bicine pH 8.5 30% glycerol/PEG 4K. The structure of A domain of CAR*ni* was solved by single-wavelength anomalous (SAD) method. Experimental phases were obtained by soaking crystals with 1M KI for 30 s before flash freezing in liquid N_2. A SAD diffraction data set was collected from a single flash-cooled crystal at Diamond light source (beamline IO4) and reflections merged and scaled with Xia2 [34]. The A domain CAR*ni* was solved using the SHELX C/D/E software package [35]. A total of 8 iodides were located (SHELX C), with sufficient phasing power to generate a heavy atom substructure (SHELX D), for phasing and density modification with SHELX E. Initial model building was done with ARP/wARP

followed by iterative cycles of manual model building and refinement in COOT [36] and with Phenix.refine [37] respectively. Structure of the A domain CAR*ni* in complex with benzoic acid was obtained by soaking the crystals in a solution of mother liquor supplemented with 0.1 M benzoic acid prior to flash-cooling.

Crystals of R domain CAR*mm* (20 mg/ml) were obtained by sitting-drop vapour diffusion in 0.2 M Na citrate tribasic dehydrate, 0.1 M Bis-tris propane pH 6.5 and 20% PEG3350. Co-crystals of CAR*mm* R domain with $NADPH_4$ were obtained in 0.2 M sodium sulphate, 0.1 M Bis-Tris-propane pH 6.5, 20% PEG3350 (SG $C222_1$) and 0.2 M ammonium tartrate dibasic, 20% PEG3350 (SG $P2_1$). Crystals were cryo-protected either in PFO oil (Hampton research) or PEG200 before flash freezing in liquid nitrogen. Structure of Red CAR*mm* was solved by molecular replacement using Phaser [35] and the NRP terminal reductase domain from *Mycobacterium smegmatis* (PDB: 4DQV).

Optimized crystals of CAR*sr* A domain (15 mg/ml) were obtained in 0.2 M calcium chloride hydrate and 20% PEG3350. CAR*sr* A-PCP (15 mg/ml) (thiolation state) crystals were grown in 1.5 M lithium sulphate and 0.1 M HEPES pH 7.5. CAR*sr* A-PCP (adenylation/reduction state) crystals were obtained in 0.2 M sodium fluoride, 0.1 M Bis-Tris Propane pH 6.5 and 20% PEG3350. CAR*sr* PCP-R crystals were obtained in the condition 0.1 M sodium malonate dibasic monohydrate, 0.1 M HEPES pH 7.0, 0.5% Jeffamine ED-2003. Sfp treated CAR*sr* PCP-R crystals were obtained in 0.1 M carboxylic acids 0.1M, 0.1M Imidazole/MES monohydrate pH 6.5, 50% ethylene glycol/PEG8K of the Morpheus screen (Molecular Dimension, UK).

All the datasets were integrated and scaled using the program XDS [38]. Structure determination of adenylation domain was done by molecular replacement using the CAR*ni* A domain as a search model. Structures of A-PCP didomain were solved by molecular replacement [39], using the A domain CAR*sr* structure as a search model. Iterative cycles of manual building in Coot [36] and refinement in Refmac [40] were used to complete the models. Iterative cycles of manual building in Coot and refinement in Refmac were used to complete the models. CAR*sr* R domain structure was solved by molecular replacement using the CAR*mm* R domain structure. Structure of CAR*sr* PCP-R didomain structure was solved by molecular replacement with refined CAR*sr* R structure and carrier protein domain from the CAR*sr* A-PCP structure.

Validation of all the structures were done with Molprobity [41] and PDB-REDO [42] were integrated into the iterative rebuild and refinement procedure. The data collection and refinement statistics for all structures are summarized in the Supplementary Table 1.

Small-angle X-ray scattering

SAXS intensity data, $I(q)$ versus q, ($q=4\pi.sin2\theta\lambda$) were collected using HPLC SAXS on beamline B21 at Diamond Light Source (Didcot, UK). 50 μL of CAR*sr* purified sample was loaded onto the Shodex KW-403 size exclusion column mounted on Agilent HPLC and the eluent was flowed though the SAXS beam at 0.15 mL/min; the buffer (25 mM Tris-Cl pH 8.0, 150 mM NaCl) used as the background was collected after one SEC column volume. SAXS data were collected at one-second intervals using a Pilatus 2M detector (Dectris,

Switzerland) at a distance of 3.9 m and an X-ray wavelength of 1 Å. All the SAXS data sets were analyzed by ATSAS [43] and Scatter suite [44]. Crysol [45] and the FoXS web server [46,47] were used to assess the fitting of SAXS data with the corresponding models. For modeling of CAR*sr* FL, A-PCP and PCP-R proteins, 10,000 independent models were generated and analyzed using EOM [48] and the results cross-validated by MultiFoxs web server [46,47].

Multi-angle light scattering and analytical ultracentrifugation

Purified CAR*sr* protein samples were injected onto a Superdex-200 10/300 GL column (GE healthcare) pre-equilibrated with 20 mM HEPES pH 7.4, 150 mM NaCl buffer for the MALS analysis. Light scattering intensities of proteins were measured at different angles relative to the incident beam and data analysis was performed with ASTRA 6 software (Wyatt Technology Corp., CA, USA). Protein fractions from MALS were then used in sedimentation velocity experiments using XL-A ultracentrifuge (Beckman Instruments) at 50,000 ×rpm (18,200 g) at 20 °C and scanning every 90 seconds respectively using a wavelength of 280 nm for a total of 200 scans. The sedimentation boundaries were analyzed using the program Sedfit v8.7 [49] and hydrodynamic radius (R_h) and frictional ratio (f/f_o) were calculated with Sednterp [50].

Stopped-flow experiments

NADPH was obtained from Sigma-Aldrich and *pro*-R and *pro*-S $NADP^2H$ were synthesized and characterized as described previously [51]. Stopped-flow studies were performed on an Applied Photophysics SX20 stopped-flow spectrometer. Experiments were conducted in 100 mM potassium phosphate buffer (pH 7.5). Before recording stopped-flow measurements CAR*mm* was activated using 10 mM $MgCl_2$, 2 mM α-methylcinnamic acid and 2 mM ATP at room temperature for 20 min. Reactions were initiated by mixing 0.5 μM NADPH (final concentration) with varied concentrations of activated enzyme, at 30 °C. For KIE measurements the same concentration of *pro*-R and *pro*-S $NADP^2H$ were mixed with the enzyme. To follow the reductive reaction, NADPH was excited at 340 nm, and emission changes were followed using a 400 nm cut-off filter.

Steady-state kinetics

The steady-state turnover of CAR*mm* at different viscosities was determined at 30 °C on assay mixtures containing 10 mM $MgCl_2$, 0.1 μM CAR*mm*, 1 mM ATP, 200 μM NADPH and 3 mM α-methyl cinnamic acid in 100 mM potassium phosphate buffer (pH 7.5). Steady-state NADPH oxidation rates were determined at 340 nm ($\varepsilon 340 = 6.22\ mM^{-1}\ cm^{-1}$) using Varian Cary 300 Bio UV-Visible Spectrophotometer. Glycerol solutions were prepared by weight and viscosity was calculated as described before [52]. ATP, NADPH and α-methylcinnamic acid concentrations were varied for respective experiments to measure apparent K_M values for CAR*mm,* CAR*ni*, nmCAR and mnCAR.

CAR biotransformation and HPLC product detection

Reactions for analysis were carried out on a 500 μL scale in a 2 mL Eppendorf. Typically, biotransformation reactions contained 5 mM substrate, 0.25 mg nickel-purified enzyme, 10

Europe PMC Funders Author Manuscripts

mM ATP, 100 mM $MgCl_2$, 10 mM NADPH in 100 mM Tris.HCl pH 7.5. The reaction contained 6.25% v/v DMSO from the addition of the substrate. The reaction was incubated at 25°C shaking at 170 rpm for 24 hr. Reactions were extracted by addition of 100 μL HPLC grade acetonitrile to 100 μL of sample, vortexed, centrifuged and filtered, samples were then analysed by HPLC. Samples to be analysed by HPLC and product conversions calculated were extracted with acetonitrile containing the 1 mg/mL 1-phenylethanol as an external standard.

Reverse phase HPLC was carried out using an Agilent 1200 Series system equipped with a G1322A degasser, G1311A Quaternary pump, G1329A standard autosampler (ALS) and a G1315B diode-array detector (DAD). All HPLC analysis was carried out using a phenomenex® HyperClone™ 5 μm ODS C18 120 Å LC column (250 × 4.6 mm). Samples were analysed using a gradient method between two solvents, Solvent **A** the aqueous phase, HPLC grade H_2O (0.1% TFA) and solvent **B** LC-MS grade acetonitrile (0.1% TFA). The initial mobile phase was 90% **A**, 10% **B**, a linear gradient was then employed over 30 min to a ratio of 30% **A**, 70% **B**, this was then returned to 90% **A**, 10% **B** over a further 10 min. Samples were run at room temperature, a sample injection volume of 10 μL, detection wavelength of 215 nm, and a flow rate of 1 mL/min were used. Conversions of products as a percentage were calculated using peak area integrations of products in ratio to the external standard 1-phenylethanol.

In order to calculate product conversion a calibration curve was performed for benzaldehyde and benzyl alcohol using the external standard 1-phenylethanol. Standards containing 1 mg/mL 1-phenylethanol and either 0.125 mg/mL, 0.25 mg/mL, 0.5 mg/mL and 1 mg/mL of benzaldehyde or benzyl alcohol were analysed by HPLC using the method described. Conversions were calculated using the linear relationship determined between the known concentration of product standards and the ratio of peak areas of these products standards and the external standard.

HPLC grade water was purchased from Romil Ltd (Cambridge, UK), Acetonitrile CHROMASOLV™ LC-MS was purchased from Honeywell Riedel-de Haën™ (Bucharest, Romania). Benzoic acid, benzaldehyde, benzyl alcohol, 1-phenylethanol, DMSO and trifluoroacetic acid were purchased from Sigma (Dorset, UK).

Data availability

Coordinates and associated structure factors have been deposited with the PDB under accession codes 5MSC, 5MSD, 5MST, 5MSS, 5MSW, 5MSR, 5MSP, 5MSV, 5MSU and 5MSO.

Supplementary Material

Refer to Web version on PubMed Central for supplementary material.

Acknowledgements

This work was supported by BBSRC grant (BB/K00199X/1 to N.T., N.S.S. and D.L.). We thank the BBSRC/EPSRC SYNBIOCHEM Centre (grant BB/M017702/1 to N.T., N.S.S. and D.L.) for access to analytical equipment.

We thank the Diamond Light Source for access to beam lines for macromolecular crystallography and bio-SAXS (proposal number MX12788). D.L. and N.T. are Royal Society Wolfson Merit Award holders. N.S.S. is an EPSRC Established Career Fellow. We thank the CoEBio3 Affiliates programme for funding to A.H.

References

1. Gross GG. Formation and reduction of intermediate aryl-adenylate by aryl-aldehyde NADP oxidoreductase from *Neurospora crassa*. Eur J Biochem. 1972; 31:585–592. [PubMed: 4405494]
2. He A, Li T, Daniels L, Fotheringham I, Rosazza JPN. *Nocardia* sp. Carboxylic Acid Reductase: Cloning, Expression, and Characterization of a New Aldehyde Oxidoreductase Family. Appl Environ Microbiol. 2004; 70:1874–1881. [PubMed: 15006821]
3. Akhtar MK, Turner NJ, Jones PR. Carboxylic acid reductase is a versatile enzyme for the conversion of fatty acids into fuels and chemical commodities. Proc Natl Acad Sci USA. 2013; 110:87–92. [PubMed: 23248280]
4. Strieker M, Tanavic A, Marahiel MA. Nonribosomal peptide synthetases: structures and dynamics. Curr Opin Struct Biol. 2010; 20:234–40. [PubMed: 20153164]
5. Gulick AM. Structural insight into the necessary conformational changes of modular nonribosomal peptide synthetases. Curr Opin Chem Biol. 2016; 35:89–96. [PubMed: 27676239]
6. Drake EJ, Miller BR, Shi C, Tarrasch JT, Sundlov JA, Allen CL, Skiniotis G, Aldrich CC, Gulick AM. Structures of two distinct conformations of holo-non-ribosomal peptide synthetases. Nature. 2016; 529:235–8. [PubMed: 26762461]
7. Riemer JM, Aloise MN, Harrison PM, Schmeing TM. Synthetic cycle of the initiation module of a formylating nonribosomal peptide synthetase. Nature. 2016; 529:239–42. [PubMed: 26762462]
8. Lennen RM, Pfleger BF. Microbial production of fatty acid-derived fuels and chemicals. Curr Opin Biotechnol. 2013; 24:1044–1053. [PubMed: 23541503]
9. Kallio P, Pasztor A, Thiel K, Akhtar MK, Jones PR. An engineered pathway for the biosynthesis of renewable propane. Nat Commun. 2014; 5:4731. [PubMed: 25181600]
10. Duan Y, Yao P, Du Y, Feng J, Wu Q, Zhu D. Synthesis of α,β-unsaturated esters via a chemo-enzymatic chain elongation approach by combining carboxylic acid reduction and Wittig reaction. Beilstein J Org Chem. 2015; 11:2245–51. [PubMed: 26664647]
11. Xu P, Qiao K, Ahn WS, Stephanopoulos G. Engineering *Yarrowia lipolytica* as a platform for synthesis of drop-in transportation fuels and oleochemicals. Proc Natl Acad Sci U S A. 2016; 113:10848–53. [PubMed: 27621436]
12. Zhou YJ, Buijs NA, Zhu Z, Qin J, Siewers V, Nielsen J. Production of fatty acid-derived oleochemicals and biofuels by synthetic yeast cell factories. Nat Commun. 2016; 7:11709. [PubMed: 27222209]
13. France SP, Hussain S, Hill AM, Hepworth LJ, Howard RM, Mulholland KR, Flitsch SL, Turner NJ. One Pot Cascade Synthesis of Mono- and Di-Substituted Piperidines and Pyrrolidines using Carboxylic Acid Reductase (CAR), ω-Transaminase (ω-TA) and Imine Reductase (IRED) Biocatalysts. ACS Catal. 2016; 6:3753–3759.
14. Finnigan W, Thomas A, Cromar H, Gough B, Snajdrova R, Adams JP, et al. Characterization of carboxylic acid reductases as enzymes in the toolbox for synthetic chemistry. ChemCatChem. 2017; doi: 10.1002/cctc.201601249
15. Gulick AM. Conformational dynamics in the Acyl-CoA synthetases, adenylation domains of non-ribosomal peptide synthetases, and firefly luciferase. ACS Chem Biol. 2009; 4:811–27. [PubMed: 19610673]
16. Chhabra A, Haque AS, Pal RK, Goyal A, Rai R, Joshi S, Panjikar S, Pasha S, Sankaranarayanan R, Gokhale RS. Nonprocessive [2 + 2]e- off-loading reductase domains from mycobacterial nonribosomal peptide synthetases. Proc Natl Acad Sci USA. 2012; 109:5681–6. [PubMed: 22451903]
17. Barajas JF, Phelan RM, Schaub AJ, Kliewer JT, Kelly PJ, Jackson DR, Luo R, Keasling JD, Tsai SC. Comprehensive Structural and Biochemical Analysis of the Terminal Myxalamid Reductase Domain for the Engineered Production of Primary Alcohols. Chem Biol. 2015; 22:1018–29. [PubMed: 26235055]

18. Marahiel MA, Stachelhous T, Mootz HD. Modular peptide synthetases involved in nonribosomal peptide synthesis. Chem Rev. 1997; 97:2651–2674. [PubMed: 11851476]
19. Thornburg CK, Wortas-Strom S, Nosrati N, Geiger JH, Walker KD. Kinetically and crystallographically guided mutations of a benzoate coa ligase (Bada) elucidate mechanism and expand substrate permissivity. Biochemistry. 2015; 54:6230–42. [PubMed: 26378464]
20. Kochan G, Pilka ES, von Delft F, Oppermann U, Yue WW. Structural snapshots for the conformation-dependent catalysis by human medium-chain acyl-coenzyme A synthetase ACSM2A. J Mol Biol. 2009; 388:997–1008. [PubMed: 19345228]
21. Kavanagh KL, Jornvall H, Persson B, Opperman U. Medium- and short-chain dehydrogenase/reductase gene and protein families: the SDR superfamily: functional and structural diversity within a family of metabolic and regulatory enzymes. Cell Mol Life Sci. 2008; 65:3895–3906. [PubMed: 19011750]
22. Awodi UR, Ronan JL, Mascchelein J, de los Santos ELC, Challis GL. Thioester reduction and aldehyde transamination are universal steps in actinobacterial polyketide alkaloid biosynthesis. Chem Sci. 2017; 8:411–415. [PubMed: 28451186]
23. Peng H, Wei E, Wang J, Zhang Y, Cheng L, Ma H, Deng Z, Qu X. Deciphering piperidine formation in polyketide-derived indolizidines reveals a thioester reduction, transamination, and unusual imine reduction process. ACS Chem Biol. 2016; 11:3278–3283. [PubMed: 27791349]
24. Mootz HD, Schwarzer D, Marahiel MA. Construction of hybrid peptide synthetases by module and domain fusions. Proc Natl Acad Sci U S A. 2000; 97:5848–53. [PubMed: 10811885]
25. Hur GH, Vickery CR, Burkart MD. Explorations of catalytic domains in non-ribosomal peptide synthetase enzymology. Nat Prod Rep. 2012; 29:1074–98. [PubMed: 22802156]
26. Calcott MJ, Ackerley DF. Portabiliy of the thiolation domain in recombinant pyoverdine non-ribosomal peptide synthetases. BMC Microbiol. 2015; 15:162. [PubMed: 26268580]
27. Khosla C, Herschlag D, Cane DE, Walsh CT. Assembly line polyketide synthases: Mechanistic insights and unsolved problems. Biochemistry. 2014; 53:2875–2883. [PubMed: 24779441]
28. Merdanovic M, Moning T, Ehrmann M, Kaiser M. Diversity of allosteric regulation in proteases. ACS Chem Biol. 2013; 8:19–26. [PubMed: 23181429]
29. Kornev AP, Taylor SS. Dynamics-driven allostery in protein kinases. Trends Biochem Sci. 40:628–647.
30. Langelier MF, Pascal JM. PARP-1 mechanism for coupling DNA damage detection to poly(ADP-ribose) synthesis. Curr Opin Struct Biol. 2013; 23:134–143. [PubMed: 23333033]
31. Dowling DP, Kung Y, Croft AK, Taghizadeh K, Kelly WL, Walsh CT, Drennan CL. Structural elements of an NRPS cyclization domain and its intermodule docking domains. Proc Natl Acad Sci U S A. 2016; 113:12432–12437. [PubMed: 27791103]
32. O'Connor SE, Walsh CT, Liu F. Biosynthesis of epothilone intermediates with alternate starter units: Engineering polyketide-nonribosomal interfaces. Angew Chem Int Ed Engl. 2003; 42:3917–3921. [PubMed: 12949868]
33. Yin J, Lin AJ, Golan DE, Walsh CT. Site-specific protein labeling by Sfp phosphopantetheinyl transferase. Nat Protoc. 2006; 1:280–285. [PubMed: 17406245]
34. Winter G, Lobley CM, Prince SM. Decision making in xia2. Acta Cryst. 2013; D69:1260–1273.
35. Sheldrick GM. Experimental phasing with SHELXC/D/E: combining chain tracing with density modification. Acta Cryst. 2010; D66:479–485.
36. Emsley P, Lohkamp B, Scott WG, Cowtan K. Features and Development of Coot. Acta Cryst. 2010; D66:486–491.
37. Adams PD, Afonine PV, Bunkoczi G, Chen VB, Davis IW, Echols N, Headd JJ, Hung LW, Kapral GJ, Grosse-Kunstleve RW, McCoy AJ, et al. PHENIX: a comprehensive Python-based system for macromolecular structure solution. Acta Cryst. 2010; D66:213–221.
38. McCoy AJ, Grosse-Kunstleve RW, Adams PD, Winn MD, Storoni LC, Read RJ. Phaser crystallographic software. J Appl Crystallogr. 2007; 40:658–674. [PubMed: 19461840]
39. Kabsch W. XDS. Acta Cryst. 2010; D66:125–132.
40. Murshudov GN, Vagin AA, Dodson EJ. Refinement of Macromolecular Structures by the Maximum-Likelihood method. Acta Cryst. 1997; D53:240–255.

41. Chen VB, Arendall WB, Headd JJ, Keedy DA, Immormino RM, Kapral GJ, Murray LW, Richardson JS, Richardson DC. MolProbity: all-atom structure validation for macromolecular crystallography. Acta Cryst. 2010; D66:16–21.

42. Joosten RP, Long F, Murshudov GN, Perrakis A. The PDB_REDO server for macromolecular structure model optimization. IUCrJ. 2014; 30:213–220.

43. Petoukhov MV, Franke D, Shkumatov AV, Tria G, Kikhney AG, Gajda M, Gorba C, Mertens HD, Konarev PV, Svergun DI. New developments in the ATSAS program package for small-angle scattering data analysis. J Appl Crystallogr. 2012; 45:342–350. [PubMed: 25484842]

44. Rambo RP, Tainer JA. Accurate assessment of mass, models and resolution by small-angle scattering. Nature. 2013; 496:477–481. [PubMed: 23619693]

45. Svergun D, Barberato C, Koch MHJ. CRYSOL - a Program to Evaluate X-ray Solution Scattering of Biological Macromolecules from Atomic Coordinates. J Appl Crystallogr. 1995; 28:768–773.

46. Schneidman-duhovny D, Hammel M, Sali A. FoXS: a web server for rapid computation and fitting of SAXS profiles. Nucleic Acids Res. 2010; 38:540–544.

47. Schneidman-duhovny D, Hammel M, Tainer JA, Sali A. FoXS, FoXSDock and MultiFoXS: Single-state and multi-state structural modeling of proteins and their complexes based on SAXS profiles. Nucleic Acids Res. 2016; 44:424–429.

48. Tria G, Mertens HDT, Kachala M, Svergun DI. Advanced ensemble modelling of flexible macromolecules using X-ray solution scattering. IUCrJ. 2015; 2:207–217.

49. Schuck P. Size-distribution analysis of macromolecules by sedimentation velocity ultracentrifugation and lamm equation modeling. Biophys J. 2000; 78:1606–1619. [PubMed: 10692345]

50. Hayes, D., Laue, T., Philo, J. Program Sednterp: Sedimentation Interpretation Program. Alliance Protein Laboratories; Thousand Oaks, CA, USA: 1995.

51. Pudney CR, Hay S, Scrutton NS. Practical aspects on the use of kinetic isotope effects as probes of flavoprotein enzyme mechanisms. Methods Mol Biol. 2014; 1146:161–175. [PubMed: 24764092]

52. Hay S, Pudney CR, Sutcliffe MJ, Scrutton NS. Are Environmentally Coupled Enzymatic Hydrogen Tunneling Reactions Influenced by Changes in Solution Viscosity? Angew Chem Int Ed. 2008; 47:537–540.

Europe PMC Funders Author Manuscripts

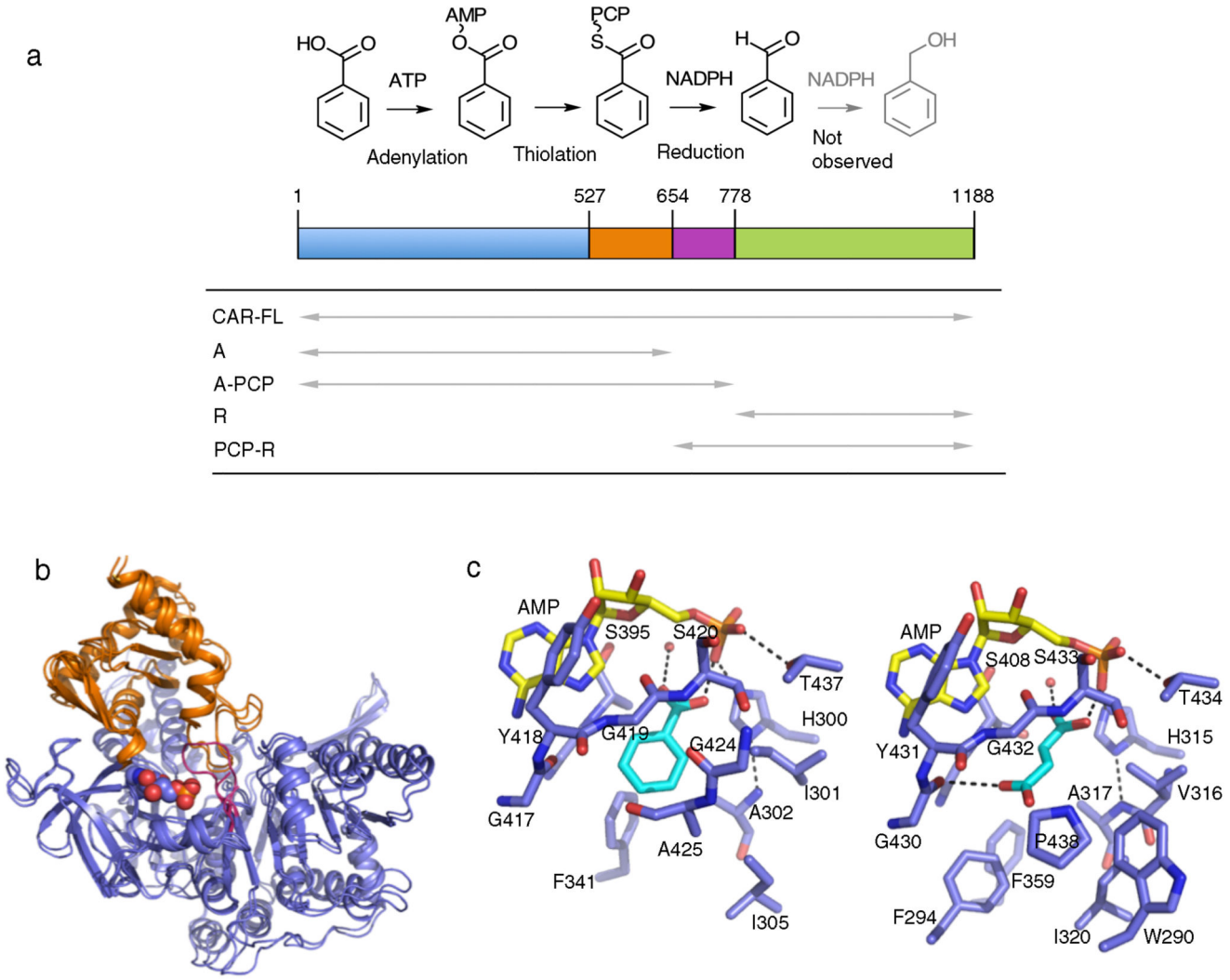

Fig. 1. Carboxylic acid reductase is a modular enzyme.

(**a**) Schematic overview of the CAR primary sequence, color coded according to individual domains. A general reaction as catalyzed by CAR is shown directly above. Various CAR fragments generated here are indicated by arrows. (**b**) An overlay of the CAR*sr* and CAR*ni* A domain crystal structures, color coded as in **a**. (**c**) A side-by-side comparison of the CAR*ni* and CAR*sr* A domain substrate-binding regions.

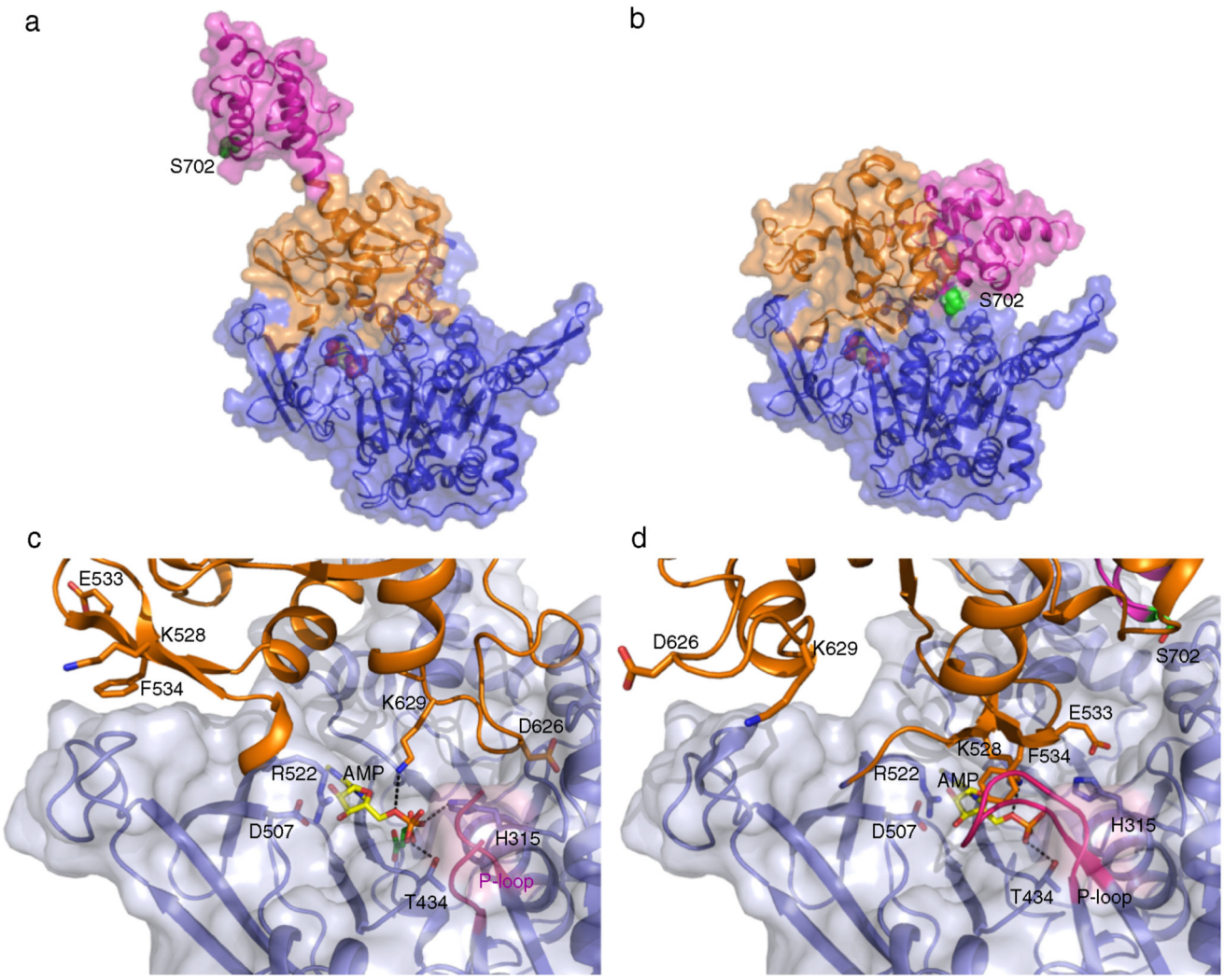

Fig. 2. Structure of the CAR*sr* A-PCP didomain reveals a dynamic entitity.

(**a**) The crystal structure of CAR*sr* A-PCP in the adenylation state. (**b**) The thiolation state crystal strucure, color coded as in Figure 1. (**c**,**d**) A detailed view of the interactions established between the AMP-bound A_{core} and the A_{sub} domain for the adenylation state (**c**) and thiolation state (**d**).

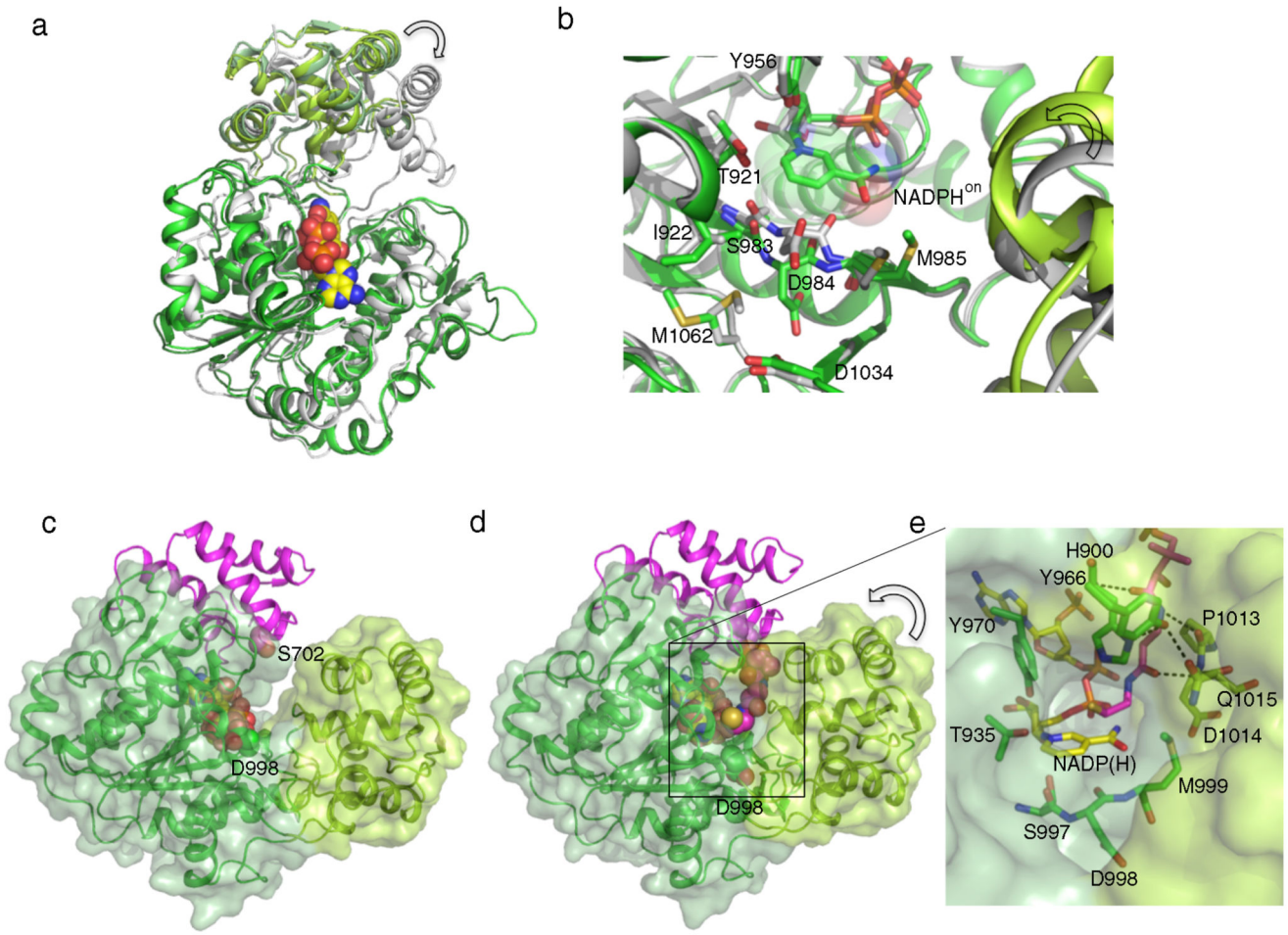

Fig. 3. Structure of CAR reductase and PCP-R regions.

(**a**) An overlay of both CAR*mm* and CAR*sr* reductase domains (dark and light green, respectively) with the related MxaA reductase domain (grey). The position of the smaller substrate binding domain is distinct for the CAR R domains, suggesting the possibility of domain motion as indicated by the arrow. (**b**) An overlay of the active site of CAR*mm* reductase in the on (light green carbons) and off (grey carbons) active site conformations. (**c**,**d**) The structures of unmodified (**c**) and phosphopantetheine-modified (**d**) CAR*sr* PCP–R didomain fragments, color coded as in Figure 1. (**e**) A detailed view of the CAR*sr* phosphopantetheine binding pocket.

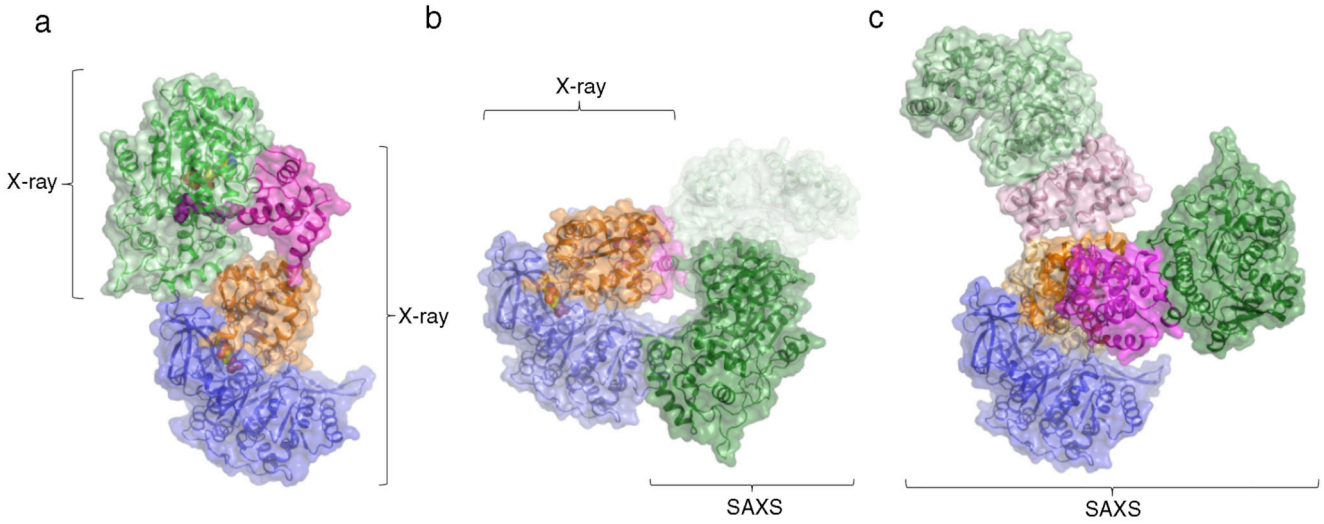

Fig. 4. Modeling of the full-length CAR structure.

(**a**) A model for the CAR*sr* acetylation/reduction state, derived from an overlay of the PCP domains of the A–PCP (acetylation state) and PCP–R crystal structures, color coded as in Figure 1. (**b**) A model for the CAR thiolation state, derived by superimposition of the A–PCP thiolation state structure with the PCP–R SAXS models. Multiple conformations of the reductase domain are shown as derived from the SAXS profile for the isolated PCP–R didomain (Supplementary Fig. 7). (**c**) The ensemble of structures that can account for the observed SAXS profile of the full length enzyme (Supplementary Fig. 8). While the individual models used can account for the observed SAXS profile of the full-length enzyme, this does not mean these are necessarily highly populated conformations.

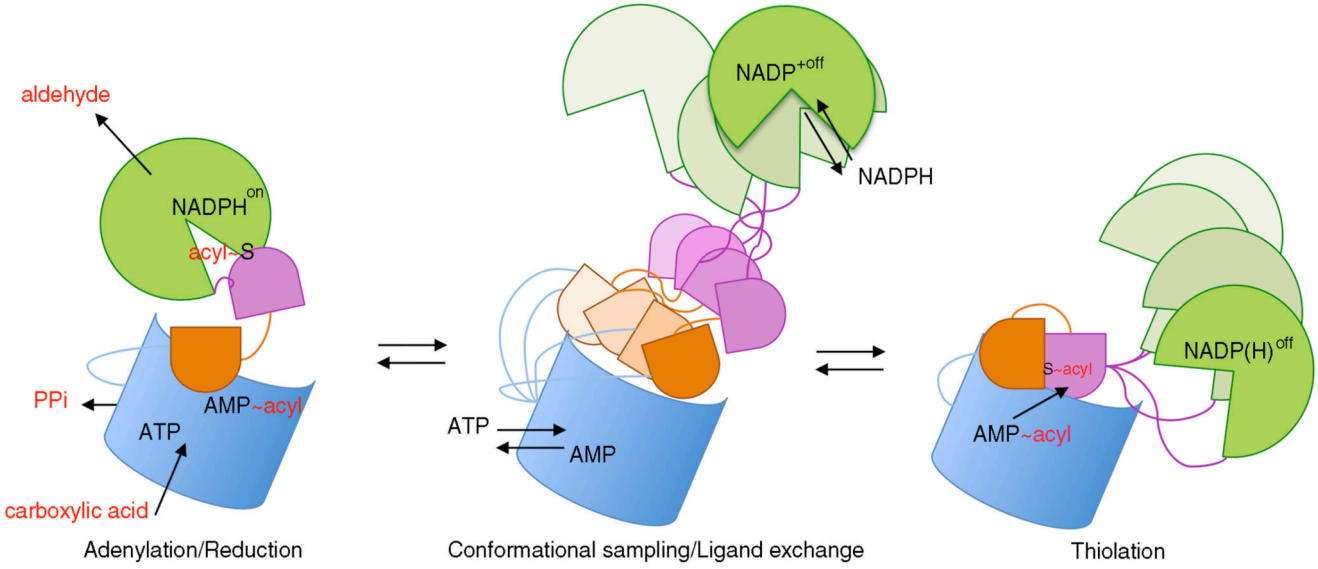

Fig. 5. A dynamic model for CAR.

A schematic representation of the conformational rearrangements during the CAR enzymatic cycle. We propose the CAR dynamic equilibrium randomly explores various conformations, some relevant with respect to catalysis, others for ligand exchange, and is not poised towards either the adenylation/reduction or thiolation conformations. In addition to the large scale reorientation of the individual domains, the reductase component displays a relatively small scale conformational equilibrium that affects the active site region and is inherently poised towards the inactive state. Docking of the phosphopantetheine group in the reductase active site leads to substrate-induced active site remodeling and activation. It is possible that reduction might occur simultaneously with activation of the next substrate molecule in the adenylation domain.

Europe PMC Funders Author Manuscripts

Europe PMC Funders Author Manuscripts

Table 1

Substrate-dependent NADPH oxidation rates (min^{-1}) for CARsr WT and variants.

A range of substrates (with or without the presence of a thiol compound) were incubated with CAR*sr*, NADPH and ATP. Substrate NAPDH oxidation rates were highest for the WT enzyme with benzoic acid, but modest activity could be observed for both full-length and individual CAR domains when using benzoyl-CoA or in the presence of (*R*)-pantetheine.

Substrates added, in addition to ATP and NADPH	Full-length CAR	CAR S702A	Apo-CAR D998G	CAR D998G	R domain	PCP–R didomain	A + PCP–R didomain
benzoic acid	278 ± 7	<0.001	<0.001	255 ± 9	<0.001	<0.001	<0.001
benzoyl-CoA	11 ± 2	3.1 ± 0.4	4.3 ± 1.6	9.4 ± 1.0	1.3 ± 1.0	2.5 ± 0.2	1.4 ± 1.2
benzoyl-CoA + (*R*)-pantetheine	ND	ND	2.7 ± 0.4	6.9 ± 0.7	ND	ND	ND
thiobenzoate	<0.001	<0.001	ND	ND	<0.001	<0.001	<0.001
benzaldehyde	<0.001	<0.001	0.15 ± 0.05	0.03 ± 0.02	ND	ND	ND
benzaldehyde + (*R*)-pantetheine	ND	ND	<0.001	<0.001	ND	ND	ND
benzoic acid + (*R*)-pantetheine	261 ± 4	6.8 ± 0.1	ND	ND	<0.001	<0.001	3.0 ± 0.8
benzoic acid + decanethiol	281 ± 11	<0.001	ND	ND	<0.001	<0.001	<0.001
benzoic acid + pentanethiol	238 ± 3	<0.001	ND	ND	<0.001	<0.001	<0.001

ND = not determined